IEEE Access
Multidisciplinary | Rapid Review | Open Access Journal

Received 13 April 2023, accepted 25 May 2023, date of publication 2 June 2023, date of current version 19 June 2023.

Digital Object Identifier 10.1109/ACCESS.2023.3282370

RESEARCH ARTICLE

An Improved Absolute-Cosine Chaotification Model and Its Simple Application in PRNG

FENG ZHANG[1], JIANENG TANG[2,3], (Member, IEEE), ZEZONG ZHANG[3], ZHONGMING HUANG[2], AND TINGTING HUANG[2]

[1]Fujian MM Electronics Company Ltd., Quanzhou 362000, China
[2]College of Engineering, Huaqiao University, Quanzhou 362021, China
[3]College of Information Science and Engineering, Huaqiao University, Xiamen 361021, China

Corresponding author: Jianeng Tang (jn_tang@hqu.edu.cn)

This work was supported in part by the National Natural Science Foundation of China under Grant 61573004, in part by the Pilot Project of Fujian Province under Grant 2022H0017, in part by the Innovation Fund Project of Fujian Province of China under Grant 2022C0037, and in part by the Quanzhou City Science and Technology Major Special Pilot Project of China under Grant 2022GZ1.

ABSTRACT Chaotic systems are widely used in various aspects such as information security, signal processing, and synchronous control. The structural complexity and the chaotic behavior of chaotic systems are two significant factors affecting their practical applications. In this paper, we propose a universal two-dimensional (2D) absolute-cosine chaotic model (ACCM). The 2D-ACCM is composed of a nonlinear bounded cosine function and an absolute value function. It can construct new chaotic maps with simple structures and complex chaotic behaviors on the basis of existing chaotic systems. To verify the effectiveness of the proposed system, we first choose two existing one-dimensional (1D) chaotic maps and one existing 2D chaotic map as the seed maps of the 2D-ACCM to generate two new maps, respectively. The results of chaotic behavior analysis show that these two new maps have more complex chaotic behavior and wider chaotic ranges than seed maps and some advanced chaotic maps. Then a hardware experiment platform based on a field-programmable gate array (FPGA) is used for the hardware implementation of the new maps. Finally, a simple chaos-based pseudo-random number generator (PRNG) is introduced to show the practical application. The experimental results show that the new maps can be easily implemented on the FPGA and the chaos-PRNGs can generate pseudo-random numbers with excellent randomness.

INDEX TERMS Chaos, chaotic behavior, 2D-ACCM, field-programmable gate array (FPGA), pseudo-random number generator (PRNG).

I. INTRODUCTION

Chaos is an important branch of nonlinear dynamics. A mathematical model that describes chaotic behavior is a chaotic system, which has many characteristics such as initial sensitivity, boundedness, ergodicity, and intrinsic randomness [1]. Because of these remarkable properties, chaos has attracted the attention of researchers. And it is widely used in various industrial applications [2], [3], including image encryption [4], [5], [6], signal processing [7], [8], secure communication [9], [10], chaotic synchronization [11], [12], etc.

Due to the wide application of chaotic systems in different fields, researchers have proposed a variety of chaotic systems. According to the form of the chaotic systems, they can be divided into two categories: discrete chaotic systems and continuous chaotic systems. For example, some classical discrete chaotic maps include the Logistic map, the sine map, the Tent map, etc. And a series of classical continuous chaotic systems include Lorenz system, Chua's circuit, etc. Similarly, according to the dimension of the chaotic systems, they can be divided into two types: high dimensional(HD) chaos and low-dimensional chaos. For example, Mansouri et al. proposed the 1D sine powered chaotic map inspired by the sine map [13]. Wang et al. designed 1D Logistic self-embedding chaotic map based on the Logistic map and the sine map [14].

The associate editor coordinating the review of this manuscript and approving it for publication was Chao-Yang Chen.

Teng et al. designed a 2D hyperchaotic map using the Logistic map and two sine maps, called 2D-CLSS [15]. Li et al. proposed a 2D conditional symmetric hyperchaotic map by introducing a polar-balanced absolute value function [16]. Zhang et al. devised a 2D lag-complex Logistic map by extending the variables of the two Logistic maps from the real to the complex domain [17]. Although so many chaotic systems have been designed by researchers, these efforts are primarily to design individual complex chaotic systems. However, there are relatively few studies on chaotic models that can generate multiple chaotic systems with good chaotic performance. And most of the chaotic models proposed by researchers are 1D systems, and there are few studies on HD chaotic models. For example, Hua et al. proposed a sine chaotification model as a general framework for improving the chaotic complexity of existing 1D chaotic maps [18]. Mansouri et al. proposed a 1D chaotic map amplifier based on the cosine function and the logarithmic function [19]. Compared with 1D chaotic maps, HD chaotic maps generally have more complex chaotic behavior, which means that they can provide good performance in practical applications. However, HD chaotic systems have disadvantages such as hardware implementation difficulties. Therefore, the development of 2D chaos is a good solution to balance the chaotic performance and practical hardware implementation.

In order to generate more chaotic systems with better chaotic performance, this paper proposes a general 2D discrete chaotic framework called the 2D absolute-cosine chaotic model (2D-ACCM). Most of the existing 2D chaotic enhancement models can only use classical 2D chaotic maps as seed maps to construct new 2D chaotic maps. However, the 2D-ACCM can use not only one existing 2D chaotic map but also two existing 1D chaotic maps as the seed map to generate a series of novel 2D chaotic systems with better performance. Theoretical analysis and experimental results show that the 2D-ACCM can effectively generate a large number of chaotic systems with better performance. The main contributions and innovations of this effort are as follows.

1) The 2D-ACCM is a general framework that can generate many 2D chaotic systems with better performance.
2) The new maps generated by 2D-ACCM have more complex chaotic behavior and wider chaotic ranges than the corresponding seed maps.
3) To verify the effectiveness of the 2D-ACCM, we first generate two new chaotic maps using two 1D chaotic maps or one 2D chaotic map as seed maps, respectively. Then the chaotic properties are analyzed by using various analysis strategies including Lyapunov exponent (LE), sample entropy (SE), correlation dimension (CD), and the sensitivity. The results show that two new maps have better chaotic performance.
4) To verify the performance of two new maps in practical applications, they are implemented on the FPGA and applied to construct a pseudo-random number generator (PRNG). The experimental results show that the new maps can be used in practical applications.

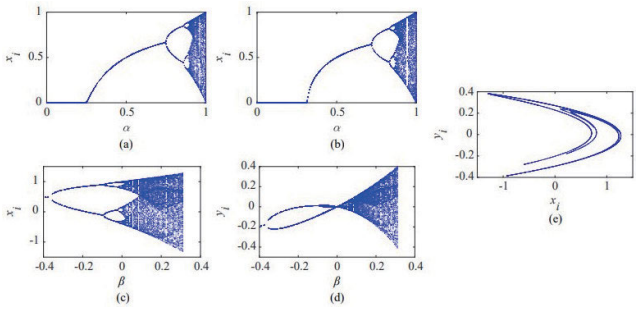

FIGURE 1. Bifurcation diagrams: (a) the Logistic map, (b) the sine map, (c) and (d) the Henon map when $\alpha = 1.4$ and $\beta \in (-0.4, 0.4)$; (e) Trajectory of the Henon map under $\alpha = 1.4$, $\beta = 0.3$.

The rest of the paper is arranged as follows. Section II reviews some existing chaotic maps and introduces the 2D-ACCM. Section III generates two new chaotic maps by using the 2D-ACCM. Section IV analyzes the chaotic performance of the new maps using LE, SE, CD, and the sensitivity. Section V discusses the hardware implementation of the new maps and their application in the PRNG. Section VI is a brief summary.

II. EXISTING CHAOTIC MAPS AND THE 2D-ACCM

This section reviews some existing chaotic maps, and introduces a new 2D discrete chaotic model called the 2D-ACCM.

A. EXISTING CHAOTIC MAPS

The Logistic map is a 1D discrete chaotic map, and its mathematical model can be written as

$$x_{i+1} = 4\alpha x_i(1 - x_i) \tag{1}$$

where $\alpha \in [0, 1]$ is the control parameter [20]. When $\alpha \in [0.89, 1]$ (approximately), the system exhibits chaotic behavior.

The sine map is a widely used unimodal map driven by a sinusoidal function, and its mathematical definition is

$$x_{i+1} = \alpha \sin(\pi x_i) \tag{2}$$

where the system parameter $\alpha \in [0, 1]$ [23]. The sine map has chaotic behavior when $\alpha \in [0.87, 1]$ (approximately).

The Henon map is a discrete 2D chaotic map. Its mathematical model is defined as

$$\begin{cases} x_{i+1} = 1 - \alpha x_i^2 + y_i \\ y_{i+1} = \beta x_i \end{cases} \tag{3}$$

where α and β are the control parameters of the Henon map [22]. When $\alpha = 1.4$ and $\beta = 0.3$, the map has chaotic behavior.

For a 1D discrete system, a bifurcation diagram is used to describe its output change with the control parameter. For a 2D discrete system, the bifurcation diagram plots the

variation of the variable x or y with the control parameters, and the trajectory represents the evolution of (x_i, y_i) when the parameters are fixed. Therefore, the bifurcation diagram and the trajectory can reflect the behaviors of the dynamic systems. The bifurcation diagrams of the Logistic map, the sine map and the Henon map, as well as the trajectory diagram of the Henon map are shown in Fig. 1.

The bifurcation diagrams show that the three classic chaotic maps all have a relatively narrow chaotic interval. At the same time, their chaotic range is not continuous, which may lead to chaotic degradation problems in practical applications. In addition, the trajectory of the Henon map shows that its output is not completely distributed, and it can only be distributed within a small interval of the phase diagram. Moreover, its trajectory is a relatively unique shape, which makes it easier to be cracked by related technologies. And these characteristics may affect their practical applications. Therefore, in order to overcome these shortcomings, it is necessary to study some systems with better chaotic behaviors.

B. THE 2D-ACCM

In order to generate more 2D discrete chaotic systems with better chaotic behaviors, we introduce a novel general 2D discrete chaotic model called the 2D-ACCM. The 2D-ACCM can use two existing 1D chaotic maps or an existing 2D discrete chaotic map as the seed map to generate a novel 2D chaotic map with better performance. The 2D-ACCM mainly includes two parts: the nonlinear cosine function and the absolute value function. And the boundedness of the cosine function makes the output of the generated 2D discrete system always bounded. Assuming that the 2D-ACCM is represented by $\mathbf{A}(x, y)$, its simple mathematical model can be defined as

$$\mathbf{A}(x_{i+1}, y_{i+1}) = \rho\pi \left|\cos[\pi(\mathbf{H}(x_i, y_i) + \theta)]\right| \tag{4}$$

where ρ and θ are the two adjustment parameters. $\mathbf{H}(x_i, y_i)$ is the seed map of the system. In order to better describe the specific mathematical definition of the 2D-ACCM, we introduce its two representations, including the 1D chaotic map as the seed map and the 2D chaotic map as the seed map, respectively.

1) THE 2D-ACCM (THE 1D CHAOTIC MAP AS THE SEED MAP)

When two 1D chaotic maps are selected as the seed map, the $\mathbf{H}(x_i, y_i)$ can be expressed as

$$\begin{cases} x_{i+1} = C_1(x_i) \\ y_{i+1} = C_2(y_i) \end{cases} \tag{5}$$

where $C_1(x)$ and $C_2(y)$ are two existing 1D chaotic maps. Thus, the 2D-ACCM can be defined as

$$\begin{cases} x_{i+1} = \rho\pi \left|\cos[\pi(C_2(y_i) + \theta)]\right| \\ y_{i+1} = \rho\pi \left|\cos[\pi(C_1(x_i) + \theta)]\right| \end{cases} \tag{6}$$

where ρ and θ are the two adjustment parameters.

2) THE 2D-ACCM (THE 2D CHAOTIC MAP AS THE SEED MAP)

When one existing 2D chaotic map is chosen as the seed map, the $\mathbf{H}(x_i, y_i)$ can be defined as

$$\begin{cases} x_{i+1} = S_1(x_i, y_i) \\ y_{i+1} = S_2(x_i, y_i) \end{cases} \tag{7}$$

where S_1 and S_2 are two iterative equations of the existing 2D chaotic map. Thus, the 2D-ACCM can be expressed by Eq. 8.

$$\begin{cases} x_{i+1} = \rho\pi \left|\cos[\pi(S_1(x_i, y_i) + \theta)]\right| \\ y_{i+1} = \rho\pi \left|\cos[\pi(S_2(x_i, y_i) + \theta)]\right| \end{cases} \tag{8}$$

Similarly, ρ and θ are the adjustment parameters.

III. TWO NEW 2D CHAOTIC MAPS

This section uses the Logistic map, the sine map and the Henon map as the seed maps to generate two new 2D chaotic maps. They are used as examples to verify the effectiveness of the 2D-ACCM.

A. THE 2D LOGISTIC-SINE MAP (2D-LS)

1) DEFINITION

A new 2D-LS map is proposed when the Logistic map and the sine map are chosen as the seed map for the 2D-ACCM. We set the adjustment parameters $\rho = 5$ and $\theta = 0.8$, and the definition of the 2D-LS is given by

$$\begin{cases} x_{i+1} = 5\pi \left|\cos[\pi(4ay_i(1 - y_i) + 0.8)]\right| \\ y_{i+1} = 5\pi \left|\cos[\pi(b\sin(\pi x_i) + 0.8)]\right| \end{cases} \tag{9}$$

where $a \neq 0$ and $b \neq 0$ are two control parameters.

2) FIXED POINTS AND STABILITY

The fixed point of a system is the element of its domain, which maps to itself. It can be simply expressed by a mathematical equation [21]. For example, it is assumed that m is fixed point of the system $\varphi(\bullet)$, then it will satisfy $\varphi(\varphi(\ldots\varphi(m)\ldots)) = m$. Therefore, the fixed point (x^*, y^*) of the 2D-LS are the root of Eq. 10.

$$\begin{cases} x^* = 5\pi \left|\cos[\pi(4ay^*(1 - y^*) + 0.8)]\right| \\ y^* = 5\pi \left|\cos[\pi(b\sin(\pi x^*) + 0.8)]\right| \end{cases} \tag{10}$$

Obviously, the Eq. 10 is a transcendental equation, and its exact numerical solution is difficult to find. Therefore, the obtained fixed points are all approximate (the accuracy of calculation is 0.0001). The change of the number of fixed points with control parameters for the 2D-LS is shown in Fig. 2(a), where a and b have the same step size of 10 ($I_a = 10$, $I_b = 10$).

The fixed point of a dynamic system usually has two states: stable and unstable. A fixed point with a stable state causes the surrounding states to be gradually attracted to the point. However, a fixed point with an unstable state causes the nearby states to gradually escape from the point, resulting in system oscillations. We can judge the stability of a fixed point

by the gradient of the system. And the gradient of the system can be represented by the eigenvalues of the system's Jacobi matrix [21]. The Jacobi matrix of the 2D-LS can be calculated as

$$J_{2D-LS} = \begin{bmatrix} 0 & P_1 \\ P_2 & 0 \end{bmatrix} \tag{11}$$

where

$$\begin{aligned} P_1 &= 5\pi^2(8ay - 4a)\sin\{\pi[0.8 - 4ay(y-1)]\} \\ &\quad \times sign\{\cos[\pi(0.8 - 4ay(y-1))]\} \\ P_2 &= -5b\pi^3\cos(\pi x)\sin\{\pi[0.8 + b\sin(\pi x)]\} \\ &\quad \times sign\{\cos[\pi(0.8 + b\sin(\pi x))]\} \end{aligned}$$

Thus, the characteristic equation can be expressed as

$$\det(\lambda E - J) = \lambda^2 - P_1P_2 = 0 \tag{12}$$

We can calculate two eigenvalues by Eq. 12: $\lambda_1 = \sqrt{P_1P_2}$ and $\lambda_2 = -\sqrt{P_1P_2}$. According to the judgment criterion of stability, the fixed point is stable when $|\lambda_1| < 1$ and $|\lambda_2| < 1$; Otherwise the fixed point is unstable. In this experiment, we can obtain $|\lambda_1| = |\lambda_2|$. And there is more than one fixed point of the system when the parameters of the system are fixed. Therefore, the calculation result of the minimum $|\lambda|$ ($|\lambda| = \min\{|\lambda_1|_1, |\lambda_1|_2, |\lambda_1|_3, \cdots, |\lambda_1|_t\}$, where the t is the number of fixed points under the same parameter) with the change of the control parameters is shown in Fig. 2(b). And it can be seen from Fig. 2(c) that the smallest value of these minimum $|\lambda|$ is about 2.58. Therefore, the results show that all the fixed points are unstable. Finally, the bifurcation diagrams and trajectory of the 2D-LS are shown in Fig. 3(a), 3(b) and 3(c), respectively. The results show that the outputs of the 2D-LS are randomly and completely distributed in the phase diagram. Therefore, it verifies the effectiveness of applying the 2D-ACCM to generate a novel 2D chaotic map with better chaotic performances.

B. THE NOVEL 2D HENON MAP (2D-NHM)

1) DEFINITION

When the Henon map is selected as the seed map of the 2D-ACCM, a new 2D chaotic map called the 2D-NHM can be gotten. The two adjustment parameters are set as $\rho = 0.5$ and $\theta = 0.8$. At this time, the 2D-NHM can be defined as

$$\begin{cases} x_{i+1} = 0.5\pi \left|\cos[\pi(1 - ax_i^2 + y_i + 0.8)]\right| \\ y_{i+1} = 0.5\pi \left|\cos[\pi(bx_i + 0.8)]\right| \end{cases} \tag{13}$$

where $a \neq 0$ and $b \neq 0$ are the two control parameters.

2) FIXED POINTS AND STABILITY

Similarly, according to the definition of the fixed point, the fixed points of the 2D-NHM is the roots of Eq. 14.

$$\begin{cases} x^* = 0.5\pi \left|\cos[\pi(1 - a(x^*)^2 + y^* + 0.8)]\right| \\ y^* = 0.5\pi \left|\cos[\pi(bx^* + 0.8)]\right| \end{cases} \tag{14}$$

Since Eq. 14 is also a transcendental equation, its exact numerical solution cannot be obtained. Here, the preset calculation accuracy is 0.0001 in the fixed point analysis and solution. The change of the number of the fixed points is shown in Fig. 2(d). The results show that the system has different numbers of fixed points under different control parameters. To judge the stability of these fixed points, the Jacobian matrix of the system is calculated as

$$J_{2D-NHM} = \begin{bmatrix} N_1 & N_2 \\ N_3 & 0 \end{bmatrix} \tag{15}$$

where

$$\begin{aligned} N_1 &= ax\pi^2\sin[\pi(1.8 - ax^2 + y)] \\ &\quad \times sign\{\cos[\pi(1.8 - ax^2 + y)]\} \\ N_2 &= -0.5\pi^2\sin[\pi(1.8 - ax^2 + y)] \\ &\quad \times sign\{\cos[\pi(1.8 - ax^2 + y)]\} \\ N_3 &= -0.5b\pi^2\sin[\pi(0.8 + bx)] \times sign\{\cos[\pi(0.8 + bx)]\} \end{aligned}$$

Therefore, the characteristic equation can be written as

$$\det(\lambda E - J) = \lambda^2 - N_1\lambda - N_2N_3 = 0 \tag{16}$$

Then, we can get the roots of the characteristic equation: $\lambda_1 = (N_1 + \sqrt{N_1^2 - 4N_2N_3})/2$ and $\lambda_2 = (N_1 - \sqrt{N_1^2 - 4N_2N_3})/2$. According to the judgment criterion of stability, it is known that the fixed point is unstable when $\max\{|\lambda_1|, |\lambda_2|\} > 1$. Therefore, in order to judge the stability of the fixed point, the larger $|\lambda|$ ($|\lambda| = \max\{|\lambda_1|, |\lambda_2|\}$) is calculated. Then the $|\lambda^*|$($|\lambda^*| = \min\{|\lambda|_1, |\lambda|_2, |\lambda|_3, \ldots, |\lambda|_t\}$) is counted, where the t is the number of fixed points under the same parameter. Finally, The values of the $|\lambda^*|$ under different parameters are shown in Fig. 2(e). Furthermore, Fig. 2(f) is a magnified view of Fig. 2(e). It can be seen that the minimum $|\lambda^*|$ is about 1.14. Therefore, the result shows that all fixed points of the 2D-NHM are unstable. In addition, the bifurcation diagrams and trajectory of the 2D-NHM are shown in Fig. 3(d), 3(e), and 3(f), respectively. The results show that the outputs of the 2D-NHM are randomly and completely distributed in the phase plane space. To sum up, the 2D-NHM has better chaotic behavior.

In order to analyze the chaotic behaviors of the new maps more objectively, the new maps are analyzed and tested by using a variety of evaluation methods in the section IV. And the results are compared with those of some advanced chaotic maps.

IV. PERFORMANCE ANALYSIS AND COMPARISON

This section analyzes the chaotic performance of two new chaotic maps using various measures including LE, SE, CD and the sensitivity. In particular, the analytical experiments are performed on MATLAB 2020b. In addition, we also compare the related properties with some existing chaotic maps including the 2D-CLSS [15], the Enhance HM [21], the Exponential sine chaotification model (ESCM) HM [22], the Logistic map, the sine map, and the Henon

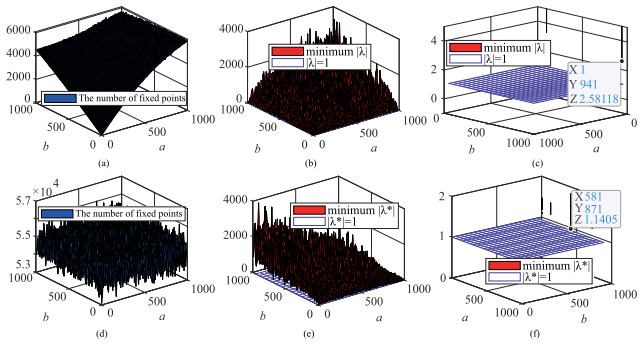

FIGURE 2. The number of fixed points and the minimum $|\lambda|(|\lambda^*|)$: (a)-(c) 2D-LS, (d)-(f) 2D-NHM.

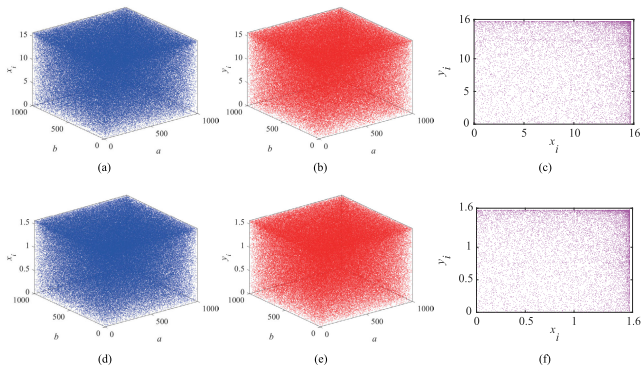

FIGURE 3. Bifurcation diagrams: (a)-(b) 2D-LS, (d)-(e) 2D-NHM; Trajectories: (c) 2D-LS with ($x_0 = 0.4$, $y_0 = 0.4$, a=50, b=50), (f) 2D-NHM with ($x_0 = 0.4$, $y_0 = 0.4$, a=50, b=50).

TABLE 1. Parameters setting of the chaotic maps.

Chaotic map	The range of parameters	Interval
Logistic	$\alpha \in [0.85, 1]$	$I_\alpha = 0.0001$
Sine	$\alpha \in [0.85, 1]$	$I_\alpha = 0.0001$
Henon	$\alpha \in [1.2, 1.4], \beta \in [0.2, 0.3]$	$I_\alpha = 0.004, I_\beta = 0.002$
Enhance HM	$a \in [1, 1000], b \in [1, 1000]$	$I_a = 10, I_b = 10$
ESCM HM	$a \in [1, 1000], b \in [1, 1000]$	$I_a = 10, I_b = 10$
2D-CLSS	$a \in [1, 1000]$	$I_a = 10$
2D-LS	$a \in [1, 1000], b \in [1, 1000]$	$I_a = 10, I_b = 10$
2D-NHM	$a \in [1, 1000], b \in [1, 1000]$	$I_a = 10, I_b = 10$

map. The simple mathematical models of the Enhance HM, the ESCM HM, and the 2D-CLSS maps can be expressed as Eq. 17, Eq. 18, and Eq. 19, respectively.

$$\begin{cases} x_{i+1} = \sin[\pi(1 - ax_i^2 + y_i)] \\ y_{i+1} = \sin(\pi b x_i) \end{cases} \tag{17}$$

$$\begin{cases} x_{i+1} = e^{\sin(\pi(1-ax_i^2+y_i))} \\ y_{i+1} = e^{\sin(\pi b x_i)} \end{cases} \tag{18}$$

$$\begin{cases} x_{i+1} = \sin[\pi(a y_i(1 - y_i))] \\ y_{i+1} = \sin[\pi(x_i + y_i)] \end{cases} \tag{19}$$

And in these experiments, their control parameters and parameter interval settings are shown in Table 1.

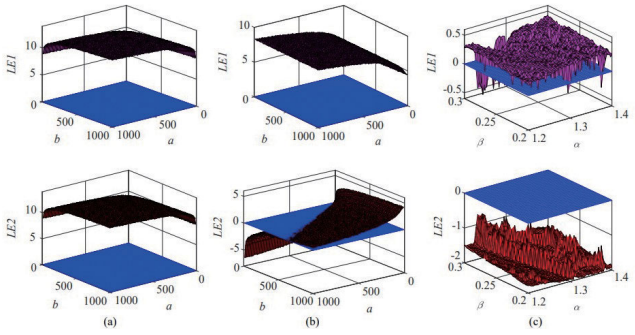

FIGURE 4. LEs: (a) 2D-LS map, (b) 2D-NHM, (c) the Henon map.

A. LE

LE is a numerical feature used to represent the average exponential divergence rate of nearby trajectories in the phase space of a dynamical system [23]. In order to analyze the objectivity of the results, we calculate the systems' LEs by using the method of the literature [24]. For a dynamic system $x_{i+1} = M(x_i)$, its Lyapunov exponent $\lambda_{M(x)}$ can be calculated by Eq. 20 [22].

$$\lambda_{M(x)} = \lim_{n\to\infty} \{\frac{1}{n} \ln \left| \frac{M^n(x_0 + \varepsilon) - M^n(x_0)}{\varepsilon} \right| \} \tag{20}$$

When a dynamical system has a positive LE value, it can be considered as a chaotic system. And if a dynamical system has no less than two positive LE values, it can be considered as a hyperchaotic system [5]. The hyperchaotic system has more complex chaotic behavior. The LEs of three chaotic maps are shown in Fig. 4. The results show that the Henon map only has positive LEs in a small parameter range, while the new chaotic maps produced by the 2D-ACCM has positive LEs in a larger parameter range. And the two new maps have two LEs greater than 0 in most parameter ranges, indicating that they exhibit hyperchaotic behavior in these ranges. Table 2 shows the average LE (ALE) and the maximum LE (MLE) for some of the existing 2D chaotic maps and three seed maps within the parameter range shown in Table 1. The results show that the proposed chaotic maps have larger LEs than the seed maps, indicating that they have more complex chaotic behavior than the seed maps. At the same time, they also have comparable chaotic behavior compared with some recently proposed sophisticated 2D chaotic maps. Therefore, the results show that the 2D-ACCM can effectively generate new 2D chaotic maps with complex chaotic behavior.

B. SE

Sample entropy is a commonly used method to measure the complexity of time series [25]. A larger positive SE value indicates a time series with lower regularity. Thus, we can evaluate the complexity of a dynamical system by judging the regularity of its output sequence. In particular, when calculating the SEs of all chaotic maps, we set the calculation parameters $m = 2$ and $r = 0.2 * std$ (std is the standard

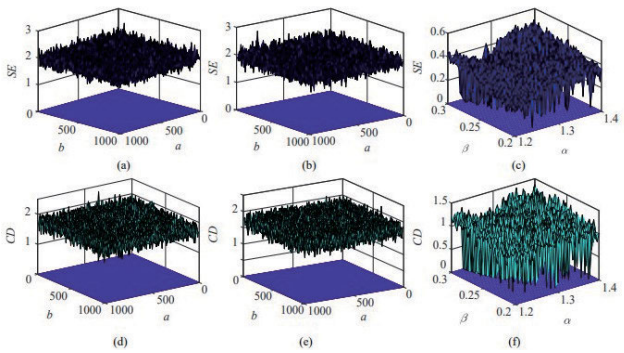

FIGURE 5. SEs and CDs: (a) and (d) 2D-LS map, (b) and (e) 2D-NHM, (c) and (f) the Henon map.

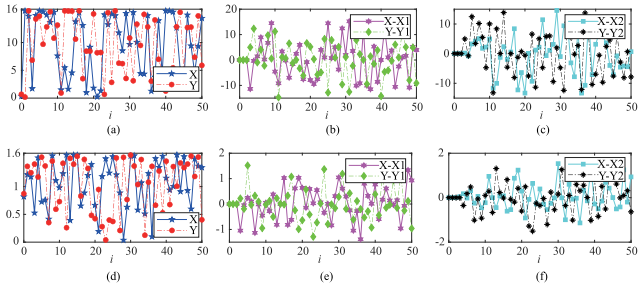

FIGURE 6. Two sequences with initial conditions (x_0, y_0, a, b): (a) 2D-LS, (d) 2D-NHM; Differences of sequences with initial conditions (x_0, y_0, a, b) and ($x_0{}^*, y_0{}^*, a, b$): (b) 2D-LS, (e) 2D-NHM; And differences of sequences with initial conditions (x_0, y_0, a, b) and (x_0, y_0, a^*, b^*): (c) 2D-LS, (f) 2D-NHM.

deviation of the test sequence) [25]. Fig. 5(a), 5(b), and 5(c) show the SE values of the two new maps and the Henon map, respectively. The results show that the two new maps have positive SE values within their entire parameter ranges and their SE values are greater than those of the Henon map. Thus, the time series generated by the two new maps have lower regularity, which indicates that they have more complex chaotic behavior. Furthermore, the maximum SE (MSE) and the average SE (ASE) of some existing 2D chaotic maps and the seed maps within their parameter ranges are shown in Table 2. The results show that the new maps have comparable complexity compared to the existing 2D chaotic maps, which further confirms the ability of the 2D-ACCM to generate complex chaotic maps.

C. CD

The CD is a kind of fractal dimension, which is widely used to measure the chaotic behavior of a system [26]. It can characterize the strange attractors of a system by evaluating the generated time series [27]. When the CD of the time series produced by a dynamic system is greater than 0, it indicates that the dynamic system has chaotic behavior. And a larger CD means that the attractor of the system occupies a higher space dimensionality. In this paper, we use the Grassberger-Procaccia (G-P) algorithm to calculate the CD [26]. The CD calculation results of the two new chaotic maps and the Henon map are shown in Fig. 5(d), 5(e), and 5(f), respectively. The results show that the new maps have positive CD values for a wide range of parameters, and the Henon maps have positive CDs only for a smaller range of parameters. Meanwhile, the average CD (ACD) and the maximum CD (MCD) of some existing chaotic maps and the seed maps are calculated as shown in Table 2. The results show that the new maps have larger average CDs than the seed maps, indicating that the new maps have more complex chaotic attractors. Moreover, the new maps have comparable average CDs compared to some existing 2D chaotic maps, which proves the effectiveness of the 2D-ACCM in generating chaotic maps with complex attractors.

D. THE SENSITIVITY

The sensitivity of chaotic systems to initial conditions is one of the most important properties. In other words, a good chaotic system must be extremely sensitive to changes of its initial conditions. Therefore, we evaluate the sensitivity of the system by observing the output sequences under different initial conditions (with very small differences). To make the experiments more rigorous, the initial conditions for each map are randomly generated in the whole range of parameters.

The experiment can be described by the following steps: First, the initial conditions are set randomly within the parameter range and are noted as $\{x_0, y_0, a, b\} = \{rand(0, 1), rand(0, 1), rand(1, 1000), rand(1, 1000)\}$, where $rand(0, 1)$ means to take a random real number in the range of [0,1]. And the chaotic sequences X and Y are generated. Second, making a minor change to the initial values x_0 and y_0, the modified initial conditions can be written as $\{x_0{}^*, y_0{}^*, a, b\} = \{x_0 + 10^{-10}, y_0 + 10^{-10}, a, b\}$, and then two new chaotic sequences X1 and Y1 are obtained. Third, making slight perturbations to the parameters a and b, the new initial conditions can be expressed as $\{x_0, y_0, a^*, b^*\} = \{x_0, y_0, a+10^{-10}, b+10^{-10}\}$, and then two new chaotic trajectories X2 and Y2 can be gotten. In particular, the above measures are used for both chaotic maps in the experiments. Fig. 6 (a) and 6(d) show the trajectories of the first 50 terms of the sequences X and Y generated by the two new chaotic maps, respectively. In addition, the trajectories of the difference values between the sequences X and X1 (X and X2, Y and Y1, Y and Y2) are also shown in Fig. 6. It can be seen that the chaotic sequences generated by the systems will gradually evolve into completely different trajectories when there is a slight change in the initial conditions. The results show that the new maps exhibit strong sensitivity to their initial values and control parameters. In addition, to quantify the sensitivity, we calculated the correlation between the chaotic sequences, and the results are shown in Table 3. The results show that the correlations between the relevant sequence pairs of the new maps are closer to 0, which indicates that the new maps have better initial sensitivity.

TABLE 2. The MLEs (MSEs, MCDs) and the ALEs (ASEs, ACDs) of the chaotic maps.

Chaotic map	The MLE		The ALE		The MSE	The ASE	The MCD	The ACD
	LE1	LE2	LE1	LE2				
Logistic	0.6930		0.1895		0.6856	0.2546	1.0371	0.6004
Sine	0.6877		0.2912		0.6924	0.3232	1.0271	0.7369
Henon	0.4316	-0.6801	0.2735	-1.6668	0.5241	0.3290	1.5017	0.9911
Enhance HM	7.4453	3.9147	6.3764	0.4192	2.2354	1.9536	2.2405	1.7073
ESCM HM	8.2808	3.7234	7.0565	-0.2750	2.4525	1.7484	2.0461	1.6468
2D-CLSS	4.0492	3.8494	3.5422	3.2674	2.3603	1.9577	2.0152	1.6853
2D-LS	12.4170	12.4365	11.3039	11.2959	2.7081	1.9480	2.3182	1.7316
2D-NHM	8.3540	4.2521	7.2658	0.4137	2.6626	1.9446	2.2522	1.7297

TABLE 3. The statistical results of correlation between trajectories.

	Random initial conditions	Original	Different initial values		Different control parameters	
		(X,Y)	(X,X1)	(Y,Y1)	(X,X2)	(Y,Y2)
Enhance HM	$(x_0, y_0, a, b) = (0.8314, 0.8034, 174, 391)$	-0.0154	0.0012	-0.0148	0.0199	-0.0134
ESCM HM	$(x_0, y_0, a, b) = (0.1067, 0.6538, 137, 722)$	-0.0069	-0.0117	-0.0067	0.0128	-0.0076
2D-CLSS	$(x_0, y_0, a) = (0.8003, 0.1419, 958)$	0.0015	-0.0286	-0.0144	-0.0035	-0.0103
2D-LS	$(x_0, y_0, a, b) = (0.3353, 0.6797, 99, 262)$	-0.0082	-0.0047	-0.0066	-0.00037	0.0039
2D-NHM	$(x_0, y_0, a, b) = (0.8182, 0.8176, 522, 97)$	0.0025	0.0059	0.00045	-0.00089	0.0027

*The length of the test sequences are 10000.

E. AUTOCORRELATION AND POWER SPECTRUM

Autocorrelation can be used to evaluate the randomness of a time series. The autocorrelation coefficient of a time series X with a length L can be expressed as

$$AC(l) = \frac{1}{L}\sum_{i=1}^{L-l} X_i X_{i+l} \tag{21}$$

For a time series that exhibits good random properties, its autocorrelation function should be approximated as the δ function. The correlation coefficient change plots for the X (Y) components of the two new maps are shown in Fig. 7. The results show that the correlation coefficient change plots are similar to the δ function, indicating that these time series exhibit relatively good random properties.

The power spectral density function is able to provide frequency domain information of a time series. The power spectra of periodic sequences have spikes at fundamental or multiplicative frequencies. However, for a chaotic sequence, the peaks of its power spectrum are connected together or have no obvious peaks. The power spectral densities of the two new maps in the X (Y) components are shown in Fig. 8. The results show that there are no significant peaks in these power spectra, indicating that these sequences exhibit chaotic performance.

V. HARDWARE IMPLEMENTATION AND PRACTICAL APPLICATION

A. HARDWARE IMPLEMENTATION

Whether a chaotic system can be implemented on a hardware platform is one of the most important factors affecting its practical application. Therefore, this section introduces the FPGA as the hardware platform to implement two new maps.

1) STRUCTURE DESIGNING

The circuit structure design for the hardware implementation of the two new maps based on the FPGA is shown in Fig.9. It mainly includes four basic modules: a startup module SETTUP, two trigonometric function computation modules Cordic1 (Cordic2) and one other computation module OCAL. The RST is an initialization input port used to initialize the system, and the SEC is a selection input port used to select the map for hardware implementation. The input ports of the four initial conditions include X_0, Y_0, CTLA, and CTLB.

2) IMPLEMENTATION RESULTS

Fig. 10 shows the hardware platform environment including an FPGA platform, a laptop, and an LCD display. The circuit designs of the two new maps are written in Verilog HDL with the simulation of Vivado 2018.3 and implemented on Xilinx FPGA Zynq Xc7z010clg400-1 using Chip scope. Finally, the output results are displayed on the LCD. In the experiment, the data format used in the experiments is defined by the IEEE 754 standard for 64-bit double precision floating point data [28]. And the initial conditions of two new maps are set to $(x_0, y_0, a, b) = (0.9, 0.3, 50, 50)$ =(3FECCCCCCCCCCCCD,3FD3333333333333,4049000000000000,4049000000000000). The hardware experiment results are shown in Fig. 11, where the top and bottom trajectories are the output sequences X and Y, respectively. In order to better observe the

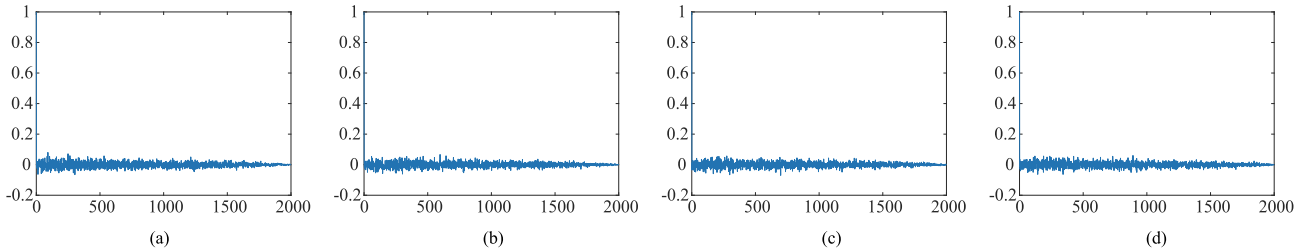

FIGURE 7. Autocorrelation coefficient: (a) 2D-LS (X), (b) 2D-LS (Y), (c) 2D-NHM (X), (d) 2D-NHM (Y).

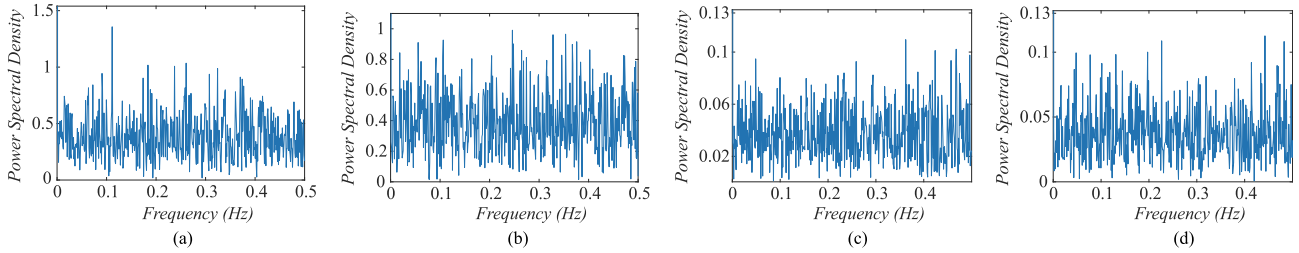

FIGURE 8. Power spectrum: (a) 2D-LS (X), (b) 2D-LS (Y), (c) 2D-NHM (X), (d) 2D-NHM (Y).

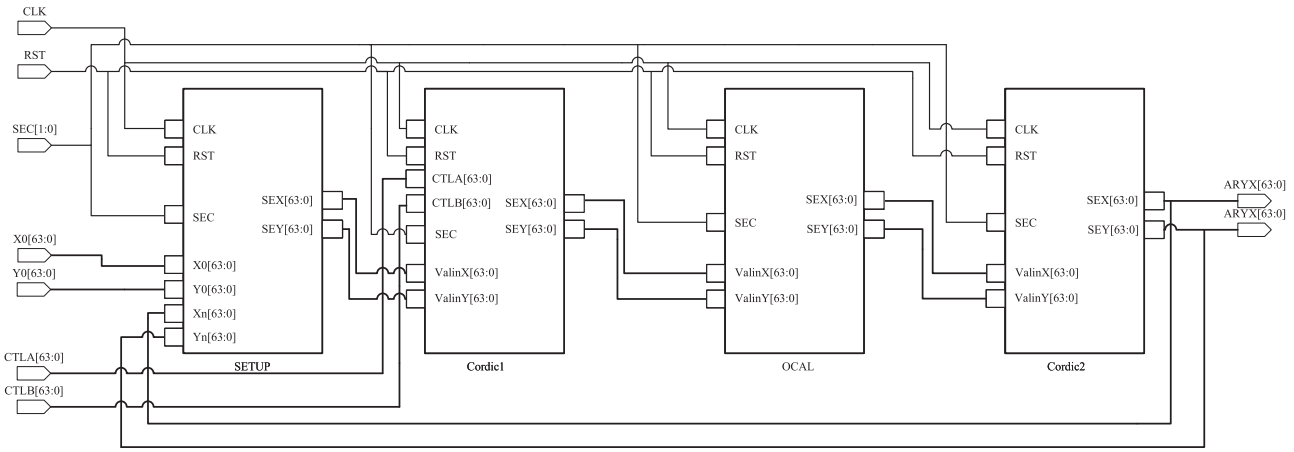

FIGURE 9. FPGA circuit structure of the chaotic maps generated by the 2D-ACCM.

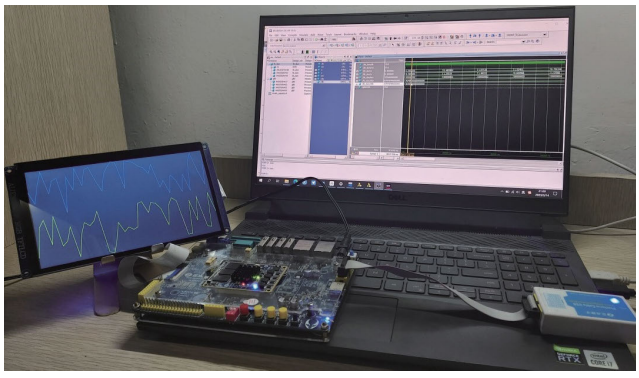

FIGURE 10. The environment for hardware implementation.

detailed values of the output data, the waveform simulation diagrams of the experiment are shown in Fig. 12.

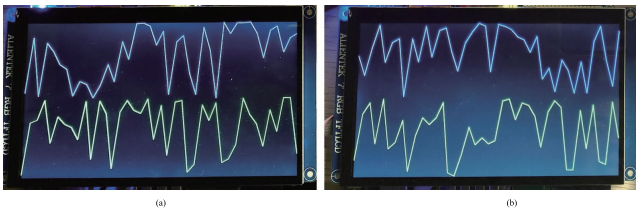

FIGURE 11. Hardware Implementation Results: (a) 2D-LS, (b) 2D-NHM.

The results show that the output sequences can be displayed correctly on the LCD screen, indicating that the new maps can be easily implemented on the hardware platform. In addition, the results of total hardware resource consumption in hardware implementation are shown in Table 4.

TABLE 4. Hardware implementation on Xilinx FPGA Zynq Xc7z010clg400-1.

Resource	Used	Available	Utilization(%)
LUT (Lookup tables)	10462	17600	59.44
LUT-RAMs (LUT-Random access memories)	510	6000	8.50
FF (Flip-Flops)	9636	35200	27.38
BRAM (Block RAM)	9.5	60	15.83
IO (Input outputs)	4	100	4.00
BUFG (Global clock buffers)	3	32	9.38

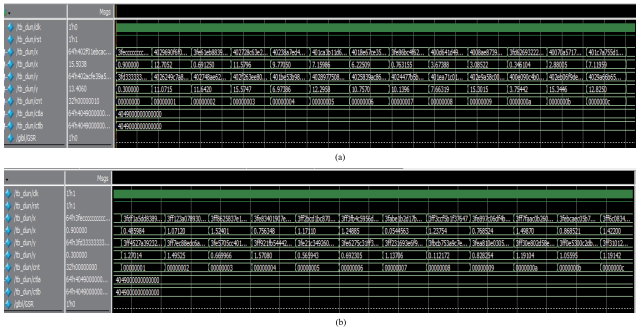

FIGURE 12. Waveform diagrams in FPGA implementation: (a) 2D-LS, (b) 2D-NHM.

B. PRACTICAL APPLICATION

Random numbers play a crucial role in a range of scientific fields such as information security, statistics and industrial simulation [29]. Due to the inherent properties of chaotic systems such as randomness and unpredictability, it is suitable for building PRNG [30]. Therefore, in this subsection, a PRNG is used to verify the practical application of the new maps.

1) PRNG DESIGNING

Suppose $X = \{x_1, x_2, \cdots, x_k\}$ and $Y = \{y_1, y_2, \cdots, y_k\}$ are the output data of the 2D chaotic map. Therefore, the proposed PRNG can be expressed as

$$P_{rng} = \lfloor \mu X + \varepsilon Y \rfloor \bmod N \tag{22}$$

where μ and ε are two larger real numbers, and P_{rng} is the generated pseudo-random number. N is a positive integer used to bound the range of the generated pseudo-random numbers to [0, N] and the function $\lfloor \bullet \rfloor$ means to obtain the largest integer that is not greater than $\bullet$. In the randomness test experiment, we set $\mu = 10^{10}$, $\varepsilon = 10^{12}$ and $N = 256$. And the control parameters a and b of the chaotic maps are randomly selected from the chaotic ranges given in Table 1, and the results of the parameters selection are shown in Table 5. The initial values are all set to $(x_0, y_0) = (0.9, 0.3)$.

2) RANDOMNESS TESTING

To verify the practical performance of the proposed PRNG, we examine the randomness of the generated pseudo-random numbers by using NIST [31] and TestU01 [32]. The software library TestU01 is widely used to measure the randomness of pseudo-random numbers [32]. In our experiment, the Rabbit, Alphabit, and BlockAlphabit test suites are used for randomness testing. And the length of the binary sequence being tested is set to 2^{30} bits, in which case the Rabbit, the Alphabit, and the BlockAlphabit include 40, 17, and 102 statistical tests, respectively. The test results of the pseudo-random sequences generated by different chaos-PRNGs are shown in Table 5. The results show that the two new maps, ESCM HM, and the Henon map can pass all tests, proving that the pseudo-random sequences generated by these PRNGs have good random properties.

TABLE 5. Parameters setting and TestU01 test results[1].

Bit length(bits)	Control parameters	Rabbit 2^{30}	Alphabit 2^{30}	BlockAlphabit 2^{30}
PRNG_(Henon)	$\alpha = 1.225, \beta = 0.292$	40/40	17/17	102/102
PRNG_(Enhance HM)	a=793,b=960	40/40	17/17	100/102
PRNG_(ESCM HM)	a=61,b=400	40/40	17/17	102/102
PRNG_(2D-CLSS)	a=656	39/40	17/17	102/102
PRNG_(2D-LS)	a=802,b=348	40/40	17/17	102/102
PRNG_(2D-NHM)	a=875,b=959	40/40	17/17	102/102

The NIST test tool includes 15 subtests. When a sequence is tested using the NIST test tool, each subtest is given a $P_{value} \in [0, 1]$. When all $P_{value} > 0.0001$, it indicates that the sequence has good random performance [33]. Table 6 shows the test results of the pseudo-random sequence generated by applying different chaotic maps to the PRNG. It is worth noting that the length of the test sequences are a series of 100 binary sequences with the length of 10^6 in the NIST test experiment. It can be seen from the table that although the P_{value} of the NIST subtests of all PRNGs are greater than 0.01, the pass rates of three PRNGs (PRNG_(Henon), PRNG_(Enhance HM), and PRNG_(2D-CLSS)) in the *NonOverlappingTemplate* subtest items fail to meet the requirements. Only PRNG_(ESCM HM), PRNG_(2D-LS), and PRNG_(2D-NHM) pass all test items, indicating that they can generate pseudorandom numbers with better random characteristics. Therefore, according to the test results of NIST and TestU01, three PRNGs including PRNG_(ESCM HM), PRNG_(2D-LS), and PRNG_(2D-NHM) are able to generate more ideal pseudorandom numbers than the other PRNGs. And the results further verify the ability of the 2D-ACCM to generate chaotic maps with good performance. In addition, compared with the two complex nonlinear structures of exponential and sinusoidal functions in the ESCM, the nonlinear structure involved in the proposed 2D-ACCM is simpler, which indicates that the proposed chaotic model consumes less resources in actual hardware implementation. Thus, the chaotic maps generated by the 2D-ACCM is more suitable for practical applications than other chaotic maps.

[1] https://github.com/pkuoo/randomness-test

TABLE 6. The results of NIST test[2].

Sub-test items	PRNG_(Henon)		PRNG_(ESCM HM)		PRNG_(Enhance HM)		PRNG_(2D-CLSS)		PRNG_(2D-NHM)		PRNG_(2D-LS)	
	Pass rate	P_{value}	Pass rate	P_{value}	Pass rate	P_{value}	Pass rate	P_{value}	Pass rate	P_{value}	Pass rate	P_{value}
Frequency	1/1	0.048716	1/1	0.816537	1/1	0.637119	1/1	0.657933	1/1	0.129620	1/1	0.366918
BlockFrequency	1/1	0.437274	1/1	0.964295	1/1	0.090936	1/1	0.191687	1/1	0.911413	1/1	0.834308
CumulativeSums*	2/2	0.181678	2/2	0.235910	2/2	0.321314	2/2	0.546123	2/2	0.668310	2/2	0.805570
Runs	1/1	0.678686	1/1	0.085587	1/1	0.191687	1/1	0.883171	1/1	0.816537	1/1	0.534146
LongestRun	1/1	0.798139	1/1	0.759756	1/1	0.719747	1/1	0.574903	1/1	0.304126	1/1	0.419021
Rank	1/1	0.419021	1/1	0.383827	1/1	0.162606	1/1	0.678686	1/1	0.162606	1/1	0.911413
FFT	1/1	0.911413	1/1	0.419021	1/1	0.171867	1/1	0.401199	1/1	0.137282	1/1	0.595549
NonOverlappingTemplate*	147/148	0.550262	148/148	0.490147	147/148	0.493165	147/148	0.527077	148/148	0.511421	148/148	0.479296
OverlappingTemplate	1/1	0.798139	1/1	0.883171	1/1	0.350485	1/1	0.987896	1/1	0.616305	1/1	0.401199
Universal	1/1	0.383827	1/1	0.474986	1/1	0.037566	1/1	0.574903	1/1	0.657933	1/1	0.224821
ApproximateEntropy	1/1	0.699313	1/1	0.249284	1/1	0.616305	1/1	0.010988	1/1	0.595549	1/1	0.719747
RandomExcursions*	8/8	0.476001	8/8	0.278382	8/8	0.344387	8/8	0.460177	8/8	0.514041	8/8	0.431590
RandomExcursionsVariant*	18/18	0.599721	18/18	0.359294	18/18	0.429471	18/18	0.610611	18/18	0.385795	18/18	0.432623
Serial*	2/2	0.398931	2/2	0.492289	2/2	0.537010	2/2	0.585909	2/2	0.558612	2/2	0.749468
LinearComplexity	1/1	0.350485	1/1	0.319084	1/1	0.574903	1/1	0.616305	1/1	0.249284	1/1	0.058984

*The average values of multiple tests.

VI. CONCLUSION

In this paper, a general 2D chaotic system is proposed called the 2D-ACCM, which can generate many new 2D chaotic maps with complex chaotic behavior based on the existing chaos. Firstly, two new chaotic maps produced by the 2D-ACCM are used as examples to evaluate the effectiveness of the 2D-ACCM. The results of the chaotic performance analysis show that compared to seed maps and some existing state-of-the-art complex 2D chaos, the new maps not only exhibit more complex chaotic behaviors but also have larger continuous chaotic intervals. Then, in order to observe the implementation of the new maps on the hardware platform, we introduce the FPGA as the hardware platform to verify the hardware implementation. Finally, a simple PRNG based on the chaos is proposed to observe the performance of the new maps in practical applications. The experiment and performance analysis results show that the new maps can be implemented relatively easily on the hardware platform, and the pseudo-random sequences generated by the chaos-PRNG have excellent random characteristics. Our future work will investigate specific applications of the new maps in areas such as information security.

REFERENCES

[1] S. S. d. Silva, M. Cardoso, L. Nardo, E. Nepomuceno, M. Hübner, and J. Arias-Garcia, "A new chaos-based PRNG hardware architecture using the HUB fixed-point format," *IEEE Trans. Instrum. Meas.*, vol. 72, pp. 1–8, 2023.

[2] X. Meng, P. Rozycki, J. Qiao, and B. M. Wilamowski, "Nonlinear system modeling using RBF networks for industrial application," *IEEE Trans. Ind. Informat.*, vol. 14, no. 3, pp. 931–940, Mar. 2018.

[3] C. E. C. Souza, D. Moreno, D. P. B. Chaves, and C. Pimentel, "Pseudo-chaotic sequences generated by the discrete Arnold's map over $Z_2{}^m$: Period analysis and FPGA implementation," *IEEE Trans. Instrum. Meas.*, vol. 71, pp. 1–10, 2022.

[4] J. Tang, Z. Zhang, P. Chen, F. Zhang, H. Ni, and Z. Huang, "An image layered scrambling encryption algorithm based on a novel discrete chaotic map," *IET Image Process.*, vol. 17, no. 2, pp. 518–532, Feb. 2023.

[5] W. Cao, Y. Mao, and Y. Zhou, "Designing a 2D infinite collapse map for image encryption," *Signal Process.*, vol. 171, Jun. 2020, Art. no. 107457.

[6] X. Wang and P. Liu, "A new full chaos coupled mapping lattice and its application in privacy image encryption," *IEEE Trans. Circuits Syst. I, Reg. Papers*, vol. 69, no. 3, pp. 1291–1301, Mar. 2022.

[7] Y. Shen, Y. Bai, T. Zou, L. Zhang, Y. Su, Z. Wu, H. Liu, and F. Yan, "Dynamical analysis of a new chaotic system and its application in ADC," *Phys. Scripta*, vol. 97, no. 8, Jun. 2022, Art. no. 085202.

[8] Z. Gao, Z. Ma, S. Wu, H. Gao, A. Wang, S. Fu, Z. Li, Y. Qin, and Y. Wang, "Physical secure key distribution based on chaotic self-carrier phase modulation and time-delayed shift keying of synchronized optical chaos," *Opt. Exp.*, vol. 30, no. 13, pp. 23953–23966, Jun. 2022.

[9] H. Chou, C. Chuang, W. Wang, and J. Lin, "A fuzzy-model-based chaotic synchronization and its implementation on a secure communication system," *IEEE Trans. Inf. Forensics Security*, vol. 8, no. 12, pp. 2177–2185, Dec. 2013.

[10] J. C. L. Chan, T. H. Lee, and C. P. Tan, "Secure communication through a chaotic system and a sliding-mode observer," *IEEE Trans. Syst., Man, Cybern., Syst.*, vol. 52, no. 3, pp. 1869–1881, Mar. 2022.

[11] P.-Y. Xiong, H. Jahanshahi, R. Alcaraz, Y.-M. Chu, J. F. Gómez-Aguilar, and F. E. Alsaadi, "Spectral entropy analysis and synchronization of a multi-stable fractional-order chaotic system using a novel neural network-based chattering-free sliding mode technique," *Chaos, Solitons Fractals*, vol. 144, Mar. 2021, Art. no. 110576.

[12] R. Zhang and S. Yang, "Robust chaos synchronization of fractional-order chaotic systems with unknown parameters and uncertain perturbations," *Nonlinear Dyn.*, vol. 69, no. 3, pp. 983–992, Feb. 2012.

[13] A. Mansouri and X. Wang, "A novel one-dimensional sine powered chaotic map and its application in a new image encryption scheme," *Inf. Sci.*, vol. 520, pp. 46–62, May 2020.

[14] X. Wang, N. Guan, and J. Yang, "Image encryption algorithm with random scrambling based on one-dimensional logistic self-embedding chaotic map," *Chaos, Solitons Fractals*, vol. 150, Sep. 2021, Art. no. 111117.

[15] L. Teng, X. Wang, and Y. Xian, "Image encryption algorithm based on a 2D-CLSS hyperchaotic map using simultaneous permutation and diffusion," *Inf. Sci.*, vol. 605, pp. 71–85, Aug. 2022.

[16] Y. Li, C. Li, S. Liu, Z. Hua, and H. Jiang, "A 2-D conditional symmetric hyperchaotic map with complete control," *Nonlinear Dyn.*, vol. 109, no. 2, pp. 1155–1165, Jul. 2022.

[17] F. Zhang, X. Zhang, M. Cao, F. Ma, and Z. Li, "Characteristic analysis of 2D lag-complex logistic map and its application in image encryption," *IEEE MultimediaMag.*, vol. 28, no. 4, pp. 96–106, Oct. 2021.

[18] Z. Hua, B. Zhou, and Y. Zhou, "Sine chaotification model for enhancing chaos and its hardware implementation," *IEEE Trans. Ind. Electron.*, vol. 66, no. 2, pp. 1273–1284, Feb. 2019.

[19] A. Mansouri and X. Wang, "A novel one-dimensional chaotic map generator and its application in a new index representation-based image encryption scheme," *Inf. Sci.*, vol. 563, pp. 91–110, Jul. 2021.

[20] R. M. May, "Simple mathematical models with very complicated dynamics," *Nature*, vol. 261, no. 5560, pp. 459–467, Jun. 1976.

[21] Z. Hua, Y. Zhou, and B. Bao, "Two-dimensional sine chaotification system with hardware implementation," *IEEE Trans. Ind. Informat.*, vol. 16, no. 2, pp. 887–897, Feb. 2020.

[22] R. Wang, M.-Y. Li, and H.-J. Luo, "Exponential sine chaotification model for enhancing chaos and its hardware implementation," *Chin. Phys. B*, vol. 31, no. 8, Aug. 2022, Art. no. 080508.

[2]https://github.com/pkuoo/randomness-test/tree/NIST

[23] Z. Zhang, J. Tang, F. Zhang, H. Ni, J. Chen, and Z. Huang, "Color image encryption using 2D sine-cosine coupling map," *IEEE Access*, vol. 10, pp. 67669–67685, 2022.
[24] A. Wolf, J. B. Swift, H. L. Swinney, and J. A. Vastano, "Determining Lyapunov exponents from a time series," *Phys. D, Nonlinear Phenomena*, vol. 16, no. 3, pp. 285–317, Jul. 1985.
[25] J. S. Richman and J. R. Moorman, "Physiological time-series analysis using approximate entropy and sample entropy," *Amer. J. Physiol.-Heart Circulatory Physiol.*, vol. 278, no. 6, pp. H2039–H2049, Jun. 2000.
[26] A. M. Albano, J. Muench, C. Schwartz, A. I. Mees, and P. E. Rapp, "Singular-value decomposition and the Grassberger-Procaccia algorithm," *Phys. Rev. A, Gen. Phys.*, vol. 38, no. 6, pp. 3017–3026, Sep. 1988.
[27] P. Grassberger and I. Procaccia, "Characterization of strange attractors," *Phys. Rev. Lett.*, vol. 50, no. 5, pp. 346–349, Jan. 1983.
[28] *IEEE Standard for Floating-Point Arithmetic*, IEEE Standard 754-2019, 2019, pp. 1–84.
[29] M. Garcia-Bosque, A. Pérez-Resa, C. Sánchez-Azqueta, C. Aldea, and S. Celma, "Chaos-based bitwise dynamical pseudorandom number generator on FPGA," *IEEE Trans. Instrum. Meas.*, vol. 68, no. 1, pp. 291–293, Jan. 2019.
[30] H. Bao, Z. Hua, H. Li, M. Chen, and B. Bao, "Discrete memristor hyperchaotic maps," *IEEE Trans. Circuits Syst. I, Reg. Papers*, vol. 68, no. 11, pp. 4534–4544, Nov. 2021.
[31] L. Bassham, A. Rukhin, J. Soto, J. Nechvatal, M. Smid, S. Leigh, M. Levenson, M. Vangel, N. Heckert, and D. Banks, "A statistical test suite for random and pseudorandom number generators for cryptographic applications," Nat. Inst. Standards Technol., Gaithersburg, MD, USA, Tech. Rep., Apr. 2010, pp. 1–131. [Online]. Available: https://tsapps.nist.gov/publication/get_pdf.cfm?pub_id=906762
[32] P. L'Ecuyer and R. Simard, "TestU01: A C library for empirical testing of random number generators," *ACM Trans. Math. Softw.*, vol. 33, no. 4, pp. 1–40, Aug. 2007.
[33] Y. Li, C. Li, S. Zhang, G. Chen, and Z. Zeng, "A self-reproduction hyperchaotic map with compound lattice dynamics," *IEEE Trans. Ind. Electron.*, vol. 69, no. 10, pp. 10564–10572, Oct. 2022.

FENG ZHANG received the B.Sc. degree in applied physics from the University of Electronic Science and Technology of China, China, in 2007.

He is currently the Deputy General Manager of Fujian MM Electronics Company Ltd. His research interests include image encryption and RF circuit design.

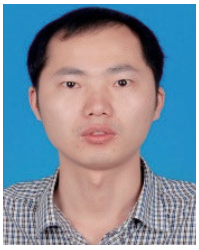

JIANENG TANG (Member, IEEE) received the M.Sc. degree in circuits and systems from Ningxia University, China, in 2009, and the Ph.D. degree in information and communication engineering from Southeast University, China, in 2012.

He is currently an Associate Professor with the College of Engineering, Huaqiao University, Quanzhou, China. He has published more than 30 papers in journals and conferences. His research interests include image encryption, RF circuit design, complex network synchronization, and chaos synchronization and control.

ZEZONG ZHANG is currently pursuing the master's degree with the College of Information Science and Engineering, Huaqiao University, Xiamen, China.

His research interests include nonlinear dynamics and control, information security, cryptanalysis, and the application of chaotic cryptography in image processing.

ZHONGMING HUANG is currently pursuing the M.S. degree with the College of Engineering, Huaqiao University, Quanzhou, China.

His research interests include information security and image privacy protection.

TINGTING HUANG received the Ph.D. degree from Xiamen University, Xiamen, China, in 2017.

She is currently a Lecturer with the College of Engineering, Huaqiao University, Quanzhou, China. Her research interests include chaotic digital communication, chaotic encryption, and ultra-wideband communications.